Journal of Environmental Management 202 (2017) 287–298

Contents lists available at ScienceDirect

Journal of Environmental Management

journal homepage: www.elsevier.com/locate/jenvman

Research article

Predicting carbon benefits from climate-smart agriculture: High-resolution carbon mapping and uncertainty assessment in El Salvador

Sean Patrick Kearney [a, *], Nicholas C. Coops [b], Kai M.A. Chan [c], Steven J. Fonte [d], Pablo Siles [e], Sean M. Smukler [a, f]

[a] Faculty of Land and Food Systems, University of British Columbia, 2357 Main Mall, Vancouver, BC V6T 1Z4, Canada
[b] Department of Forest Resource Management, 2424 Main Mall, University of British Columbia, Vancouver, V6T 1Z4, Canada
[c] Institute for Resources, Environment and Sustainability, University of British Columbia, 2202, Main Mall, Vancouver, V6T 1Z4, Canada
[d] Department of Soil and Crop Sciences, Colorado State University, 1170 Campus Delivery, Fort Collins, CO 80523, USA
[e] International Center for Tropical Agriculture, Km 17 Recta Cali-Palmira, Apartado Aéreo 6713, Cali, 763537, Colombia
[f] Tropical Agriculture Program, The Earth Institute at Columbia University, 61 Route 9W, Lamont Hall, Room 2H, Palisades, NY 10964-8000, USA

ARTICLE INFO

Article history:
Received 10 March 2017
Received in revised form
12 July 2017
Accepted 15 July 2017
Available online 22 July 2017

Keywords:
Aboveground biomass carbon
Smallholder agriculture
Ecosystem services
Landscape
Remote sensing
Uncertainty

ABSTRACT

Agroforestry management in smallholder agriculture can provide climate change mitigation and adaptation benefits and has been promoted as 'climate-smart agriculture' (CSA), yet has generally been left out of international and voluntary carbon (C) mitigation agreements. A key reason for this omission is the cost and uncertainty of monitoring C at the farm scale in heterogeneous smallholder landscapes. A largely overlooked alternative is to monitor C at more aggregated scales and develop C contracts with groups of land owners, community organizations or C aggregators working across entire landscapes (e.g., watersheds, communities, municipalities, etc.). In this study we use a 100-km^2 agricultural area in El Salvador to demonstrate how high-spatial resolution optical satellite imagery can be used to map aboveground woody biomass (AGWB) C at the landscape scale with very low uncertainty (95% probability of a deviation of less than 1%). Uncertainty of AGWB-C estimates remained low (<5%) for areas as small as 250 ha, despite high uncertainties at the farm and plot scale (34–99%). We estimate that CSA adoption could more than double AGWB-C stocks on agricultural lands in the study area, and that utilizing AGWB-C maps to target denuded areas could increase C gains per unit area by 46%. The potential value of C credits under a plausible adoption scenario would range from $38,270 to $354,000 yr^{-1} for the study area, or about $13 to $124 ha^{-1} yr^{-1}, depending on C prices. Considering farm sizes in smallholder landscapes rarely exceed 1–2 ha, relying solely on direct C payments to farmers may not lead to widespread CSA adoption, especially if farm-scale monitoring is required. Instead, landscape-scale approaches to C contracting, supported by satellite-based monitoring methods such as ours, could be a key strategy to reduce costs and uncertainty of C monitoring in heterogeneous smallholder landscapes, thereby incentivizing more widespread CSA adoption.

1. Introduction

Multiple benefits can be realized at both the farm and landscape scale when managing for carbon (C) storage in smallholder agriculture (Harvey et al., 2013). Benefits include reduced erosion, increased habitat and biodiversity, improved nutrient cycling and yield stability (Steenwerth et al., 2014); however, due to a variety of methodological concerns related to C monitoring, international and voluntary agreements on land-use-related C mitigation have largely omitted agriculture, and have instead been restricted to reforestation and afforestation activities (Pelletier et al., 2012; Turnhout et al., 2017). Agroforestry management can store substantial amounts of C in aboveground woody biomass (AGWB; e.g., Henry et al., 2009) and soil (Lorenz and Lal, 2014). It is considered a form of "climate-smart agriculture" (CSA) because it can serve to both mitigate climate change through increased terrestrial C storage and increase the

* Corresponding author. The University of British Columbia, 2424 Main Mall, Vancouver, BC V6T 1Z4, Canada.
E-mail addresses: sean.kearney@alumni.ubc.ca (S.P. Kearney), nicholas.coops@ubc.ca (N.C. Coops), kaichan@ires.ubc.ca (K.M.A. Chan), steven.fonte@colostate.edu (S.J. Fonte), p.siles@cgiar.org (P. Siles), sean.smukler@ubc.ca (S.M. Smukler).

http://dx.doi.org/10.1016/j.jenvman.2017.07.039
0301-4797/

resilience of agricultural systems (e.g., through the benefits mentioned above), thereby improving farmers' ability to adapt to an already changing climate (Steenwerth et al., 2014; Verchot et al., 2007).

There is growing interest in including CSA practices like agroforestry in C mitigation programs (e.g., Harvey et al., 2013; Steenwerth et al., 2014), and efforts are underway to develop strategies to monitor C sequestration associated with changes in smallholder agricultural land management (Gómez-Castro et al., 2010; Henry et al., 2009; Marinidou et al., 2013; Rosenstock et al., 2016). Small farms sizes, low C sequestration rates per hectare and inaccessibility in smallholder landscapes often result in unacceptably high costs when attempting to monitor C at the farm scale (Cacho et al., 2013). This not only hampers efforts to assess the C mitigation benefits of CSA, but has also led some authors to conclude that agroforestry-based C contracts with individual farmers would likely be impractical at current C prices (Henry et al., 2009; Luedeling et al., 2011).

An alternative is to develop C contracts with groups of landholders or organizations at the landscape scale (e.g., the scale of watersheds, communities, municipalities, etc.), rather than with individual farmers. This approach offers several potential benefits: 1) reduced monitoring and transaction costs and uncertainty if C accounting occurs at more aggregated scales rather than on individual farms; 2) increased flexibility for communities to promote or incentivize CSA for multiple benefits, beyond just C storage (Harley et al., 2012); and 3) the ability to achieve C storage through a suite of interventions (e.g., agroforestry, fire management, afforestation and reforestation), allowing activities to be dynamic and meet the needs of individual land managers and communities within the same contract (Chhatre and Agrawal, 2009; Harley et al., 2012; Stringer et al., 2012).

A key step to developing landscape-scale C contracts is the development of accurate C monitoring methods at aggregated scales (Scherr et al., 2012), especially for C stored in AGWB. The simplest and most common methods to estimate landscape AGWB-C are inventory-based or 'stratify and multiply' approaches (Goetz et al., 2009). Specifically, these approaches involve assigning a single C value, or a range of values, to individual vegetation, thematic or land use/land cover (LULC) classes, which are then multiplied by class areas estimated from satellite imagery, existing maps, census data or other sources. Such approaches face challenges for monitoring changes in AGWB-C from CSA adoption, especially in smallholder landscapes (Kearney and Smukler, 2016). For example, CSA practices exist along a gradient, confounding binary definitions of what is and is not CSA, thus complicating assignation of specific C values to each LULC class. Furthermore, calculating LULC class area totals is exceptionally challenging in smallholder landscapes due to small field sizes, highly heterogeneous management practices, shifting cultivation and rapid changes in land use over time.

Monitoring approaches utilizing remote sensing data to develop wall-to-wall AGWB-C maps show promise to overcome the challenges of 'stratify and multiply' approaches in smallholder landscapes, although with limitations (Gibbs et al., 2007). AGWB estimations from passive optical satellite sensors have generally been considered too uncertain to meaningfully monitor AGWB-C due to a variety of complications such as biomass saturation effects and highly heterogeneous landscapes resulting in mixed-pixels (Goetz and Dubayah, 2011; Ravindranath and Ostwald, 2008; Zolkos et al., 2013). However, increasing spatial resolution of imagery and advanced processing techniques are yielding improved accuracy in estimating AGWB-related vegetation parameters from optical satellite imagery. For example, the accuracy of optically-derived AGWB estimations has been improved by incorporating texture variables representing the structural arrangement of surfaces within prediction models (Castillo-Santiago et al., 2010; Eckert, 2012; Fuchs et al., 2009; Kayitakire et al., 2006; Sarker and Nichol, 2011).

While uncertainty of AGWB-C predicted from optical imagery may remain high at the pixel and plot scale, it can be markedly reduced when aggregated across a landscape due to the spatial scaling of uncertainty. For example, several studies have shown that uncertainty of AGWB predictions from remote sensing is lower at more aggregated scales, either as a result of increasing map grain size (Asner et al., 2010; Lusiana et al., 2014; Mascaro et al., 2011a) or by aggregating across larger areas (Asner et al., 2010; Fazakas et al., 1999; Saatchi et al., 2011). However, little discussion has been given to the overall uncertainty of landscape AGWB totals derived from very high spatial resolution optical imagery and how it relates to monitoring efforts for C payments and CSA.

The aim of this study was to assess how landscape-scale C mapping can overcome monitoring challenges for C contracting in regions dominated by smallholder agriculture, with an application to a mountainous region of El Salvador. Our objectives were therefore to (1) investigate the potential for using high resolution optical satellite imagery to quantify AGWB-C stocks in a smallholder landscape at multiple scales, accounting for uncertainty, (2) quantify expected gains in AGWB-C with the adoption of CSA and potential payments for C credits and (3) explore the benefits of using remote sensing to target low-biomass areas to promote agroforestry in smallholder landscapes.

2. Materials and methods

Our analytical framework to realize the aforementioned objectives consisted of four main steps. First, we took field measurements of individual trees in 0.1 ha plots to calibrate high-spatial resolution QuickBird satellite imagery acquired coincident with field measurements. Second, we mapped AGWB-C for the entire study area using a multiple linear regression model developed from a suite of potential predictor variable extracted from the QuickBird image and a digital elevation model (DEM). Third, we estimated the uncertainty of our AGWB-C map at multiple scales using two methods: a simple quadratic scaling approach and an object-weighted approach to account for spatial autocorrelation. Finally, we predicted expected changes in AGWB-C for the study area for several scenarios of CSA adoption and estimated potential gross value of C credits at different market prices. We describe each of these steps in detail below.

2.1. Description of the study area

The study area (Fig. 1) encompasses a 100-km^2 (10,000 ha) area within an association of seven municipalities in El Salvador known as La Mancomunidad La Montañona (hereafter referred to as La Mancomunidad). La Mancomunidad is a mountainous mosaic of mixed-pine forest (*Pinus oocarpa* and *Quercus* spp.), broadleaf secondary forest/fallow patches and widespread agricultural activity dominated by subsistence smallholder cultivation of basic grains (maize, beans and sorghum) and extensively grazed pastures. The Ministry of Environment and Natural Resources of El Salvador (MARN) identified this area as a priority region for testing and promoting improved agricultural management due to the predominance of basic grain farming and small-scale livestock on steep slopes near a protected forest area. Elevations range from 265 to 1,575 m and the region has a sub-humid tropical climate with a mean annual temperature of 22–26°C and mean annual rainfall of about 1,985 mm (MARN, 2013). Rainfall occurs mostly between the months of May and October with a pronounced dry season from November to April, averaging less than 10 mm month^{-1} between

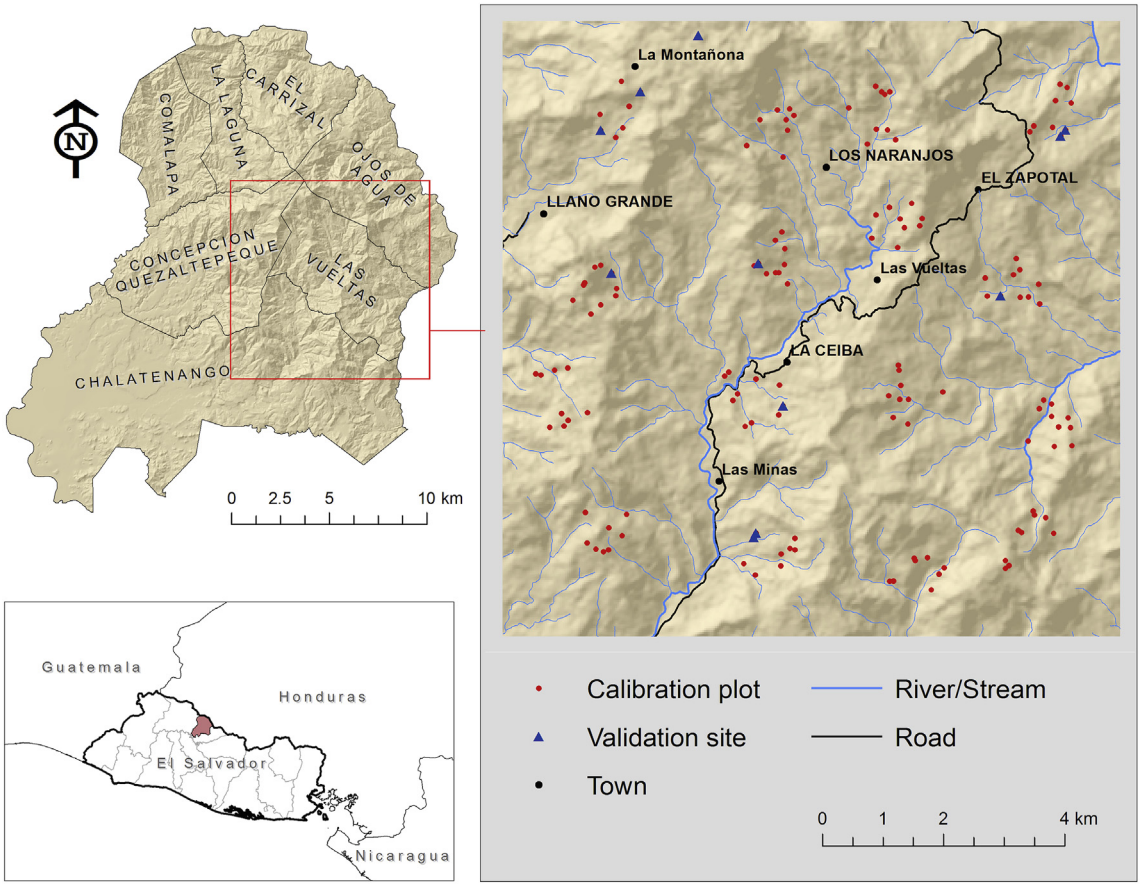

Fig. 1. Map of the 10,000 ha study area (inset) within the seven municipalities known as La Mancomunidad La Montañona (location shown in pink on the overview map). (For interpretation of the references to colour in this figure legend, the reader is referred to the web version of this article.)

December and February.

2.2. Data collection

A total of 138 circular calibration plots, each with a radius of 17.84 m (area of 0.1 ha), were sampled in late 2012 utilizing a hierarchical sampling method following a modified version of the Landscape Degradation Surveillance Framework (LDSF) (Shepherd et al., 2015). Initial site selection was carried out utilizing the LDSF method, but plot centers were 'pushed' a random distance at a randomly chosen angle into the nearest homogenous land use parcel when the plot lay within multiple land uses. Plot centers were then georeferenced using GPS and differentially corrected to permanent base towers, achieving sub-meter accuracy for all locations.

Species, height and diameter at breast height (DBH) were measured for all trees with DBH $\geq$ 10 cm. The same measurements were taken for trees with DBH 1–10 cm in a 0.01 ha circular subplot in the plot center. Eleven larger plots in the study area were surveyed in early 2013 as part of a regional landscape survey encompassing all of La Mancomunidad. Ten of these sites were agricultural fields ranging in size from 0.19 to 0.89 ha that encompassed randomly selected calibration plots and the eleventh was a 1-ha mixed-pine forest plot. These plots were used as validation sites to compare predicted map uncertainty to observed prediction error.

A high-spatial resolution QuickBird satellite image (0.6 m panchromatic, 2.4 m 4-band spectral) of the study area was acquired on December 4, 2012. The ASTER 30-m DEM was also downloaded.

2.3. Mapping AGWB-C

AGWB was calculated for each tree within the sample plots from a combination of species-specific and generalized allometric equations using DBH, height and, when necessary, wood-specific gravity values from the literature (see Supplementary Materials). AGWB-C was estimated as 49% of AGWB based on several studies throughout Central America (Gómez-Castro et al., 2010; Hughes et al., 1999; Suárez, 2002). AGWB-C density was calculated in metric tons per hectare (Mg ha^{-1}) by summing the estimated AGWB-C of each tree within the plot and converting to a per-hectare area basis.

We used plot data to develop a contiguous prediction map of AGWB-C for the entire study area using a multivariate linear regression model developed from a suite of potential predictor variables derived from the QuickBird and ASTER DEM datasets (Table 1). Predictor variables were identified from similar studies using multiple linear regression models to estimate AGWB from optical imagery and are listed in Table 1, along with their sources, when applicable. All variables were created in ArcGIS 10.1 (ESRI, 2011) or ENVI 5.1 (Exelis Visual Information Solutions, 2010) and their mean and/or standard deviation values extracted for each 0.1 ha plot.

An exhaustive search was used to test all possible regression model subsets with the *leaps* package (Lumley, 2009) in R, Version 2.9 (R Core Team, 2016). The dependent variable, AGWB-C, was approximately log-normally distributed and was log transformed after adding a constant of 1 to each value to avoid issues with zero values. The maximum number of predictor variables allowed was capped at seven (a sample size to variable ratio of roughly 20:1) and

Table 1
Potential predictor (independent) variables tested in the stepwise multivariate linear regression model. N = the number of variables for each variable type.

Variable type	Name	Description/equation	Data/equation source
Individual Bands (mean & standard deviation) N = 8	Band 1 (Blue)	450-520 nm	DigitalGlobe
	Band 2 (Green)	520-600 nm	
	Band 3 (Red)	630-690 nm	
	Band 4 (NIR)	760-900 nm	
	Panchromatic	450-900 nm	
Band Ratios N = 6	NIR/Blue	B4/B1	(Okubo et al., 2010)
	Red/Blue	B3/B1	
	Green/Blue	B2/B1	
	NIR/Green	B4/B2	
	Red/Green	B3/B2	
	NIR/Red	B4/B3	
Vegetation Indices N = 6	EVI	$2.5\ \frac{NIR-Red}{(NIR+6*Red-7.5*Blue)+1}$	(Jensen, 2005)
	NDVI	$\frac{NIR-Red}{NIR+Red}$	(Jensen, 2005)
	ARI2	$NIR\left[\frac{1}{Green}-\frac{1}{Red}\right]$	(Exelis Visual Information Solutions, 2010)
	ARVI	$\frac{NIR-[Red-(Blue-Red)]}{NIR+[Red-(Blue-Red)]}$	(Jensen, 2005)
	OSAVI	$\frac{1.5*(NIR-Red)}{(NIR+Red+0.16)}$	(Exelis Visual Information Solutions, 2010)
	SR	$\frac{Red}{NIR}$	(Jensen, 2005)
Tasseled Cap N = 4	TC 1	Brightness	(Yarbrough and Easson, 2005)
	TC 2	Greenness	
	TC 3	Wetness	
	TC 4	Fourth Coordinate	
Principal Components N = 4	PC 1	Principal components 1–4	(Exelis Visual Information Solutions, 2010)
	PC 2		
	PC 3		
	PC 4		
GLCM Texture Variables N = 35	Contrast	Individual bands (Bands 1–4 with 11 × 11 pixel window; Panchromatic with 25 × 25 pixel window)	(Exelis Visual Information Solutions, 2010)
	Correlation		
	Dissimilarity		
	Entropy		
	Homogeneity		
	Second Moment		
	Variance		
Ratios of GLCM Texture Variables N = 28	Contrast	Band Ratios with 11 × 11 pixel window (B4/B2; B4/B3; B3/B4; B3/B2)	(Sarker and Nichol, 2011)
	Correlation		
	Dissimilarity		
	Entropy		
	Homogeneity		
	Second Moment		
	Variance		
Terrain N = 4	Elevation	meters above sea level (m.a.s.l.)	NASA
	Slope	degrees	(ESRI, 2011)
	Insolation	Solar radiation tool, ArcGIS 10.1	(ESRI, 2011)
	TWI	$TWI = \ln\left(\frac{a}{\tan B}\right)$ where, a = upslope contributing area (m^2) and B = slope (degrees).	(Wilson and Gallant, 2000)

the 40 best model subsets for each number of independent variables were selected using the Bayesian information criterion (BIC) and adjusted-R^2, resulting in 280 potential models. Finally, the variance inflation factor (VIF) was calculated for each of the 280 potential models and all models with a VIF greater than 10 were removed due to high potential multicollinearity (García et al., 2010; Nichol and Sarker, 2011). Of the remaining models, the one with the lowest BIC and highest adjusted R^2 was selected as the final regression model and checked for heteroscedasticity and normality of residuals.

A correction value was calculated to correct for bias introduced by the log-transformation of the dependent variable following methods described in Sprugel (1983). The cross-validated root mean square error (RMSE-CV) of the final model was then evaluated using leave-one-out cross validation (LOOCV) with the *DAAG* package (Maindonald and Braun, 2015) in R.

In order to generate the final prediction map, a mean filter using a circular moving window set at a radius of 17.84 m (equal to the plot area of 0.1 ha) was applied to a raster of each independent variable in the final model to account for the fact that the model was built using mean values of 0.1 ha plots. These filtered rasters were used to create a prediction map of log-transformed AGWB-C for each pixel, which was then back-transformed and corrected to produce a final AGWB-C prediction map.

2.4. Estimating map uncertainty

The uncertainty of aggregated AGWB-C was estimated at multiple scales as the 95% confidence interval in Mg of AGWB-C. Uncertainty was first calculated for each pixel using the following equation:

$$C_{Px} \pm U_{Px} = t_{\left(1-\frac{\alpha}{2},\, \boldsymbol{df}\right)} * SE_{Px} \quad (1)$$

where C_{Px} is the predicted AGWB-C at pixel Px, U_{Px} is the uncertainty at pixel Px, t is the Student t critical value at a specified alpha (α) and degrees of freedom (df) (in this case $\alpha = 0.05$ and $df = 131$) and SE is the standard error of prediction at pixel Px. The lower and upper uncertainty values for each predicted AGWB-C value were then calculated by back-transforming the lower and upper confidence interval limits, respectively, and calculating the difference

from the predicted value for each pixel. Due to back-transformation, this results in asymmetrical lower and upper uncertainty values. Therefore, average uncertainty was also calculated for each pixel as the simple average of the two values.

Aggregate uncertainty was calculated in two ways (with and without accounting for spatial autocorrelation) at multiple scales to explore how uncertainty changes as the size of the aggregation unit varies from plot to farm to landscape scale. Lattice grids ranging from approximately 0.01 to 10,000 ha on a logarithmic scale were created for the entire study area and the average aggregate uncertainty calculated for each grid as the mean percent uncertainty of individual grid cells.

Aggregate uncertainty was first calculated for each grid as the quadratic sum of all pixels within an aggregation unit as

$$C_A \pm U_A = \sqrt{\sum_{n=1}^{Px} U_{Px}^2} \quad (2)$$

where C_A is the aggregate AGWB-C (calculated as the sum of predicted pixel values within the aggregation unit), U_A is the aggregate uncertainty and U_{Px} is the uncertainty at pixel Px, as calculated in Eq. (1). This method is a simple way to estimate uncertainty where under- and over-prediction are equally likely for each individual pixel, and has been used by others to aggregate uncertainty for AGWB predictions (Asner et al., 2010; Saatchi et al., 2011). However, since the quadratic sum method assumes errors are independent and random (Palmer, 2003), it does not account for potential spatial autocorrelation within the data. While no spatial autocorrelation was detected in the residuals of the 138 calibration plots, it may potentially occur at the pixel scale (i.e., at distances much smaller than that between most calibration plot pairs) and, as a result, an object-weighted approach was developed to account for local spatial autocorrelation.

The object-weighted approach consisted of three basic steps: (1) calculate the effective range of spatial autocorrelation of pixel prediction uncertainty, (2) segment the image into spatial objects with similar uncertainty and (3) weight the sum of uncertainty based on the average distance between points within each object, up to the effective range identified in step 1.

In order to calculate the effective range, a variogram was produced from the prediction uncertainty map using the *gstat* package in R (Pebesma, 2004). The very high-spatial resolution of the uncertainty map made it computationally expensive to compute a variogram for the entire study area at once, therefore the map was resampled to 9.6 m pixels and a bootstrapping approach was used to construct variograms for 1000 randomly selected subsections of approximately 1 × 1 km each. The results of these 1000 individual variograms were averaged to produce a single estimate of the semivariance between cells, to which an exponential model was fit. The exponential model yielded an effective range of 281 m, beyond which spatial autocorrelation of uncertainty is assumed to be inconsequential (Fig. S1).

The original 2.4 m uncertainty map was then segmented using ENVI 5.0 (Exelis Visual Information Solutions, 2010) and the average distance between cells within each object calculated as

$$D_o = e^{(0.5*\log(A_o)-0.6515)} \quad (3)$$

where D_o is the average distance between points within an object (o), and A_o is the area of the object. The sum of prediction uncertainty of pixels within each object was weighted using a modification of Equation (2), where the exponent is scaled between 1 and 2, such that within each object,

$$C_o \pm U_o = \sqrt[S_o]{\sum_{n=1}^{Px} U_{Px}^{S_o}} \quad (4)$$

and S_o is calculated as

$$S_o = 1 + D_o\left(\frac{1}{281}\right) \quad (5)$$

In this manner, uncertainty of very small objects was aggregated by the near-arithmetic sum (i.e., assuming near-perfect spatial autocorrelation), whereas uncertainty was scaled toward the quadratic sum for very large objects where the average distance between pixels exceeded the effective range of 281 m (i.e., assuming independence of errors). The weighted uncertainty of each object was then summed in quadrature for each aggregation unit according to Equation (2), since objects are by definition assumed to be independent of each other.

2.5. Predicting changes in AGWB-C with CSA adoption and potential C value

Simple scenarios of expected AGWB-C gains with the adoption of CSA practices were created to examine the potential magnitude and value of C storage in the study area. Scenarios were based on the objectives of several recent and ongoing projects in La Mancomunidad to promote CSA for multiple benefits, including storing AGWB-C. Specifically, the CSA practices of interest include the adoption of a slash-and-mulch agroforestry system (e.g., Hellin et al., 1999) and improved silvopasture management (e.g., Dagang and Nair, 2003), both typified by increasing the number and diversity of managed trees left in fields and pastures, thus increasing AGWB-C stocks.

Predicted gains in AGWB-C with conversion from conventional management to CSA were estimated from expected changes in tree density and size-distribution. Based on recommendations from experts and on-farm trials, the average target tree density and size-distribution for the CSA practices of interest is approximately 100 large trees (DBH 10–40 cm) and 1000 small trees (DBH 5–10 cm) per hectare, respectively. When converted to basal area, this equates to a target basal area averaging 9.33 m^2 ha^{-1}, which agrees well with the limited published observations of basal area in mature agroforestry and silvopasture systems in Central America (e.g., Pauli et al., 2011). Using simple linear regression with data from ground plots in cropland, pasture and broadleaf secondary forest/fallow in this study (n = 127), the relationship between basal area and AGWB-C was modeled, yielding an estimated target AGWB-C of 23.35 Mg ha^{-1} ± 0.69 Mg ha^{-1} (one standard error) at the target basal area of 9.33 m^2 ha^{-1}.

A LULC map was overlaid with the predicted AGWB-C map to identify areas currently under cropland, pasture or broadleaf secondary forest/fallow classes where AGWB-C gains would be realized with conversion to CSA (i.e., areas with predicted AGWB-C less than 22.51 Mg ha^{-1}). We note that predicted AGWB-C gains in broadleaf secondary forest/fallow classes are likely an underestimate, since we maintain the simple assumption that fallows will retain 22.51 Mg C ha^{-1} coming out of agroforestry/silvopasture, ignoring additional gains from tree growth that would come as the fallow matures. For each pixel identified, the predicted gain in AGWB-C with CSA adoption was calculated using a Monte Carlo simulation where, for each iteration,

$$G_i = C_i - T_i \quad (6)$$

and G_i is the predicted gain in AGWB-C in Mg ha^{-1} for the ith

iteration, C_i is current AGWB-C in Mg ha^{-1} randomly chosen from the distribution of possible predicted values for each pixel and T_i is the target AGWB-C with CSA adoption, which was randomly chosen from a normal distribution with a mean of 22.51 Mg ha^{-1} and a standard deviation of 0.82 Mg ha^{-1} (derived from our model results). The simulation was conducted 100 times and total AGWB-C gain for the study area was calculated for each iteration. The median was taken as the expected total gain in AGWB-C and the 2.5th and 97.5th percentiles used to calculate a 95% confidence interval. We took the lower bound of this interval as the minimum expected gain in AGWB-C with conversion from conventional management to CSA across the study area.

We estimated the minimum expected gain in AGWB-C under three adoption scenarios: 1) full adoption (100% of all agricultural land converted to CSA), 2) 50% adoption randomly distributed across agricultural lands and 3) 50% adoption targeting only the most denuded areas (i.e., areas with expected gains of at least 5 Mg C ha^{-1}). For each scenario, minimum expected gain was calculated using a probability distribution function (PDF) to estimate the gain we expect could be monitored with 95% confidence based on the uncertainty of the prediction map.

Finally, the potential value of C-payments for CSA adoption was estimated to contextualize the potential for developing a community-scale C contract over a 15-year period. Gross C value (not accounting for monitoring and transaction costs) was calculated by multiplying the minimum expected gain in AGWB-C (converted to metric tons of CO_2 equivalents) by the market price for C. We did this for three different prices of CO_2 equivalents, since prices are highly variable across markets and over time. We chose prices of $4 per ton (the approximate low for EU Allowance credits in 2013), $12 per ton (the approximate price of California Carbon Allowance Futures from 2014 to 2016) and $37 per ton, the 'social' or 'shadow' price of carbon as estimated by the US Interagency Working Group on the Social Cost of Carbon (US Interagency Working Group on the Social Cost of Carbon, 2015).

3. Results

3.1. Mapping AGWB-C

AGWB-C density in the 138 calibration plots ranged from 0 to 92 Mg C ha^{-1} and, as anticipated, varied by land use (Table 2). Variability was high in all LULC classes, and highest for cropland and pasture.

Of the 280 AGWB-C calibration models 149 met the model selection criteria. GLCM texture variables, namely *correlation, entropy* and *homogeneity* from the panchromatic image and Bands 1 and 3, were the most frequently selected variables (Fig. 2). The ratio of the Second Moment of Band 4 to Band 3 was the only GLCM texture ratio consistently selected. In general, vegetation indices, terrain variables, tasseled cap transformations, PCA and ratios of GLCM texture variables were rarely included in model subsets. Models with more variables generally had lower BIC and higher adjusted R^2. No models with seven variables passed the multicollinearity threshold (VIF < 10). Three models with 6 variables met the VIF threshold but did not pass tests for normality of residuals. Therefore, the final chosen model based on the selection criteria contained 5 variables with an adjusted R^2 of 0.52, RMSE-CV of 16.38 Mg ha^{-1} (81.71%) and a correction factor of 1.38 (Table 3).

The final map of predicted AGWB-C corresponded well with known areas of high biomass, for example the intact mixed-pine forest in the northwest of the study area, broadleaf riparian zones along rivers and streams and the less-populated highlands in the southeast (Fig. 3). Map uncertainty (as percent of the prediction value) was typically highest in image-shadowed areas and areas with very low biomass (Fig. 4). Based on the sum total of all pixels in the prediction map, aggregate AGWB-C for the study area is estimated at 257,360 Mg, about 8.8% higher than a simple plot-based estimate calculated using a 'stratify and multiply' approach (Table 4). Overall average AGWB-C density was 25.81 Mg ha^{-1} and estimates of average AGWB-C density by LULC class were similar to plot-based averages.

Table 2
Select descriptive statistics for aboveground woody biomass carbon (AGWB-C) in calibration plots by land use/land cover LULC class (CROP = cropland, PAST = pasture, BLF = broadleaf secondary forest/fallow, MPF = mixed-pine forest). CV is the coefficient of variation.

LULC class	n	AGWB C (Mg C ha^{-1})				CV
		Mean	Median	Min	Max	
CROP	29	9.73	3.48	0.00	60.22	1.38
PAST	44	11.3	8.75	0.00	35.62	0.87
BLF	52	27.33	24.77	1.57	70.66	0.66
MPF	13	43.48	40.87	13.08	91.92	0.52
OVERALL	**138**	**20.04**	**15.26**	**0.00**	**91.92**	**0.93**

3.2. Estimating map uncertainty

The grid simulation showed an exponential decay in prediction uncertainty as the size of aggregation units increased for both calculation methods (Fig. 5). However, prediction uncertainty for smaller aggregation units was markedly lower using the quadratic sum of individual pixel uncertainty compared to the object-weighted approach.

At the scale of sample plots (0.1 ha) and farms (~1 ha), the object-weighted approach predicted uncertainties of about 50–100%, which was nearer to the range of observed prediction error for most validation plots compared to the quadratic sum (Fig. 5). Object-weighted uncertainty declined below 5% for aggregation units larger than about 250 ha. At the scale of the study area (10,000 ha), uncertainty was less than 1% using both methods.

3.3. Predicting changes in AGWB-C with CSA adoption and potential C value

Expected gain in AGWB-C with full conversion to CSA practices within the study area is 58,920 Mg, or about 28% of the estimated total in managed land uses. Of this potential gain, 19,510 Mg (33%) comes from conversion of cropland to agroforestry, 26,760 Mg (45%) from pasture to silvopasture and 12,650 Mg (21%) from increased AGWB-C in broadleaf secondary forest/fallow resulting from higher AGWB-C in managed lands entering back into forest/fallow uses (Table 5). Overall, nearly 60% of the land area not currently under mixed-pine forest could see gains in AGWB-C with CSA adoption. Nearly all cropland and pasture areas have potential to increase AGWB-C, while we would expect to see gains in 36% of the area classified as broadleaf secondary forest.

Combining the uncertainty of the expected gain with the uncertainty of the aggregate AGWB-C, we estimate that a minimum gain of 57,340 Mg could be measured with 95% confidence with 100% adoption of CSA. With 50% adoption by random farms (simulating a non-targeted approach) the expected measurable gain drops to 26,770 Mg. However, the expected AGWB-C gains are not evenly distributed and targeting areas with high potential gain, as shown in the map below (Fig. 6), was expected to yield substantially higher C gains than a random non-targeted approach. Indeed, with 50% adoption targeting only the most denuded areas, measureable landscape AGWB-C gains jumped to 39,110 Mg, about 46% higher than the random approach (Table 6).

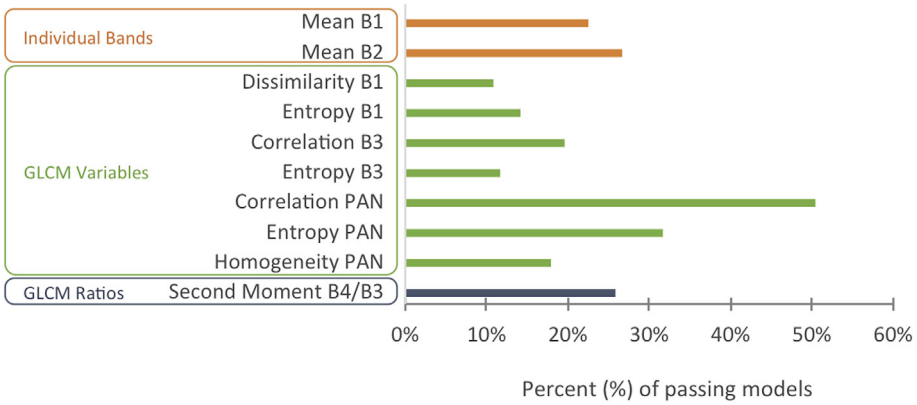

Fig. 2. Top 10 most frequently chosen variables occurring in the models that met the model selection criteria (n = 183).

Table 3
Results for the final model subset chosen. CF is the correction factor (see Sprugel, 1983) and VIF is the variance inflation factor.

Variable	Coefficient est.	Std. error	Pr (>|t|)	VIF
Intercept	−1.67985	1.35761	0.218	
Band 1	−0.03174	0.00698	<0.001	1.92
Entropy (Band 3)	−0.00669	0.00129	<0.001	2.62
Correlation (Panchromatic)	8.12406	1.19259	<0.001	2.02
Entropy (Panchromatic)	1.26736	0.27321	<0.001	3.06
Second Moment (NIR/Red)	5.26955	1.14585	<0.001	3.89
Adjusted R^2 = 0.52 | RMSE-CV = 16.38 Mg ha^{-1} (81.71%) | CF = 1.3810				

We estimate that AGWB-C would increase by nearly 40,000 Mg, or 143,500 tons CO_2 equivalent, with a 50% adoption rate over a 15-year period targeting the most denuded agricultural areas (Table 6). Depending on the price per metric ton CO_2 equivalent, the gross value of C gains ranged from $574,000 (at $4 per ton) to as much as $5,310,000 (at $37 per ton) for the study area. Annual gross value of C per hectare of land converted to CSA ranged from $13–124 ha^{-1} yr^{-1}, equivalent to between 2.6 and 25.3% of average net on-farm profits in the study area (estimated at $491 ha^{-1} yr^{-1}, data not shown).

4. Discussion

4.1. Mapping AGWB-C

We find that AGWB-C in this region is relatively low, consistent with other estimates for degraded tropical landscapes dominated by smallholder agriculture. Saatchi et al. (2011) mapped tropical forest

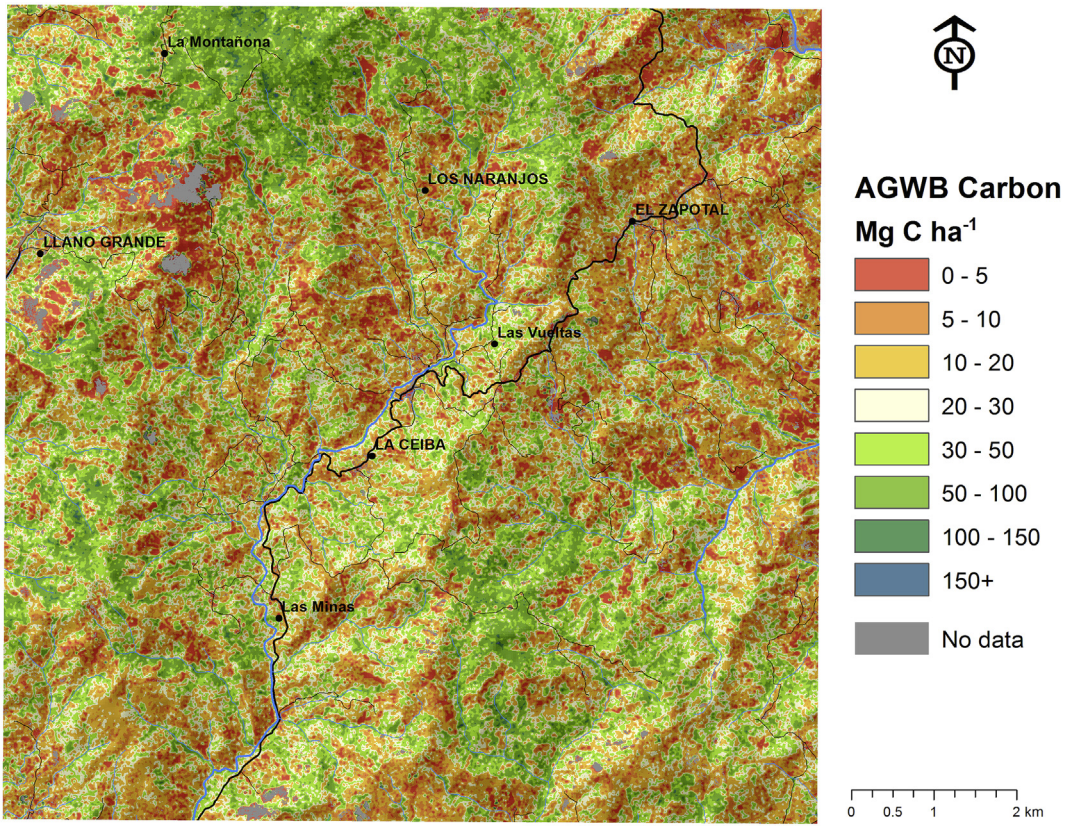

Fig. 3. Final map of predicted AGWB-C at 2.4 m resolution. 'No data' areas in grey are due to cloud cover.

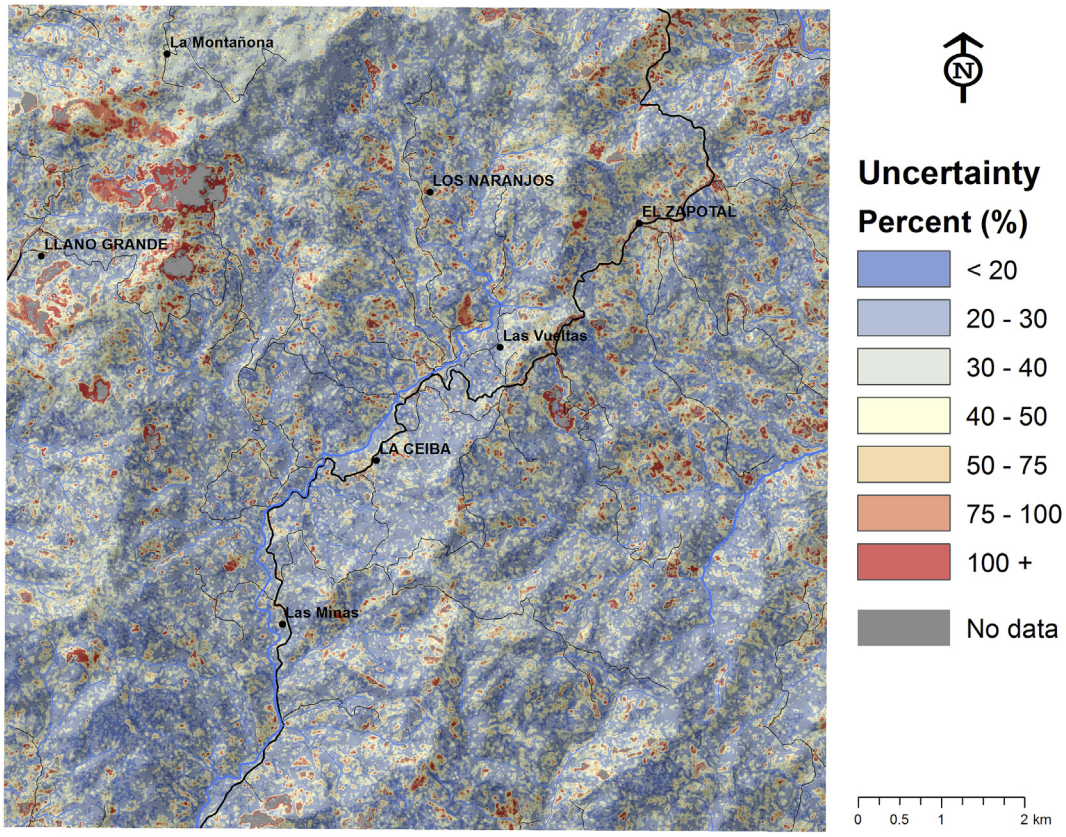

Fig. 4. Percent uncertainty of AGWB-C predictions, calculated as the percent of the predicted value using the average error of the upper and lower bounds of the 95% confidence interval. 'No data' areas in grey are due to cloud cover.

Table 4
Estimated aboveground woody biomass carbon (AGWB-C) totals and per-hectare means by land use/land cover (LULC) class (CROP = cropland, PAST = pasture, BLF = broadleaf secondary forest/fallow, MPF = mixed-pine forest).

LULC Class	Map area	Map-based		Plot-based	
		Total	Mean	Total	Mean
	(ha)	(Mg)	(Mg ha^{-1})	(Mg)	(Mg ha^{-1})
CROP	1,680	20,610	12.27	16,360	9.73
PAST	2,217	27,800	12.54	25,410	11.46
BLF	5,218	165,700	31.75	157,270	30.14
MPF	854	43,250	50.65	37,400	43.81
OVERALL	9,970	257,360	25.81	236,440	22.63

C stocks at the national scale across Latin America, sub-Saharan Africa and Southeast Asia and estimated average AGWB-C density in forests in El Salvador to be between 39 and 60 Mg C ha^{-1}, within the measured range for broadleaf secondary forest and mixed-pine forest in this study. Hughes et al. (1999) found similar results for secondary forests in a Mexican smallholder landscape. Total AGWB-C ranged from 2 to 50 Mg C ha^{-1} in young secondary forests (<15 yrs) and 44–146 Mg C ha^{-1} in secondary forests $\geq$ 15 yrs (assuming that 50% of total AGWB in their study is C).

Our results demonstrate that a multiple-linear regression model applied to high-resolution satellite imagery can provide accurate estimates of aggregate AGWB-C for a highly heterogeneous and degraded (low-biomass) smallholder landscape, even with relatively small calibration plots (0.1 ha). Some studies have suggested that AGWB estimates from passive optical imagery alone are too uncertain to satisfy monitoring guidelines (Zolkos et al., 2013). However, our findings show that optical imagery calibrated with a large number of relatively small plots offers a promising option for monitoring AGWB-C aggregated across large areas (greater than ~250 ha) with very low uncertainty (less than 5%). This is encouraging as small sample plots are not only less costly but in fact necessary in these fragmented landscapes where homogenous land-use units are irregularly shaped and frequently less than 1 ha.

The ranges of map uncertainty and observed errors at the scale of a typical farm (0.1–1 ha) suggest that monitoring AGWB-C in individual fields may not be feasible using the methodology presented in this study. However, map uncertainty seems to correspond reasonably well with observed error, implying that the predicted 95% confidence interval for aggregate AGWB-C will usually encompass the true aggregate AGWB-C, even in farm-size plots.

Uncertainty estimates reported in the literature often refer only to the fit of the model used to predict AGWB, usually by the root mean squared error (RMSE) or the mean absolute error (MAE) (Castillo-Santiago et al., 2010; Eckert, 2012; Fuchs et al., 2009; Tsui et al., 2013). The RMSE and MAE are simple and common methods for reporting the uncertainty of a prediction map (Sexton et al., 2015), but they are derived at the scale of the sample unit used to build the model and do not necessarily represent the uncertainty of aggregated total AGWB-C in a landscape (Mascaro et al., 2011b). Our method utilizing spatially explicit uncertainty estimates and statistical aggregation demonstrates that the uncertainty of landscape predictions can be quite low, and that for areas less than about 10,000 ha spatial autocorrelation of uncertainty should be incorporated, but for larger areas simple quadratic scaling may be appropriate.

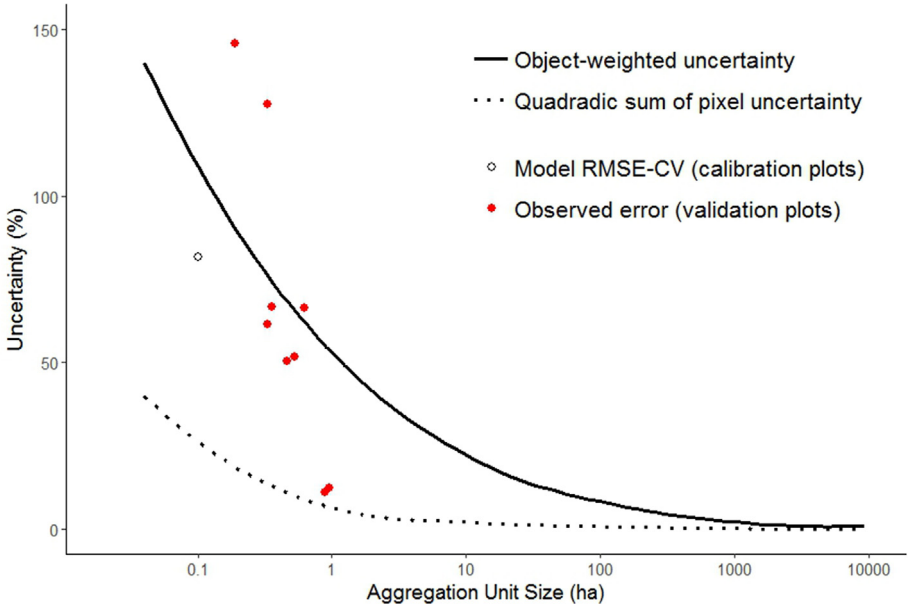

Fig. 5. Aggregated aboveground woody biomass carbon (AGWB-C) prediction uncertainty by aggregation unit size. The dotted line shows average uncertainty by plot size from the grid simulation calculated as the quadratic sum of pixel uncertainty and the solid line shows the object-weighted uncertainty. The open circle represents the cross-validated root mean squared error (RMSE-CV) from the 0.1 ha calibration plots (n = 138), and filled red circles show observed error in validation plots. NOTE: Two of the validation plots were excluded from the figure to improve readability, but are included in the Supplementary Materials (Table S4). Percent error in these two plots was very high (>300%) despite low gross AGWB-C error (<3 Mg) due to dividing by a small measured C value for the plot (<2 Mg). (For interpretation of the references to colour in this figure legend, the reader is referred to the web version of this article.)

Table 5
Potential gain in aboveground woody biomass (AGWB-C) by land use/land cover (LULC) class with 100% adoption of CSA (CROP = cropland, PAST = pasture, BLF = broadleaf secondary forest/fallow).

LULC Class	Area with AGWB-C gain	Percent of LULC class map area	Average density gain	Expected total gain	Percent gain (compared to current total)[a]	Percent of expected total gain
	(ha)	%	Mg C ha^{-1}	Mg C	%	%
CROP	1560	92.64%	12.53	19,510	94.66%	33.12%
PAST	2010	90.43%	13.29	26,760	96.25%	45.42%
BLF	1860	35.61%	6.80	12,650	0.08%	21.46%
OVERALL	5430	59.47%	10.85	58,920	27.52%	100.00%

[a] Based on current totals by LULC class as calculated from the map prediction averages.

Only a few other studies have explored how uncertainty in AGWB varies with the size of aggregation units. Asner et al. (2010) discussed how map error declines precipitously with increasing sample area and with increasing grain size, falling to 4–5% at 5 ha resolution, and Mascaro et al. (2011b) found similar results for grain sizes ranging from 0.04 ha to 6.25 ha. Lusiana et al. (2014) showed lower uncertainty of C emissions with larger pixel sizes, dropping from 82% error at 1 ha resolution to below 5% at 100 ha. Saatchi et al. (2011) found that tropical biomass C estimates aggregated at the national scale had uncertainties around 1% and remained bounded to within ±5% when aggregated to 10,000 ha using 1 km^2 (100 ha) pixels. Fazakas et al. (1999) mapped forest biomass in Sweden using a Landsat TM image and found that while the RMSE at the plot scale (~0.03 ha) was around 70%, uncertainty fell to < 10% when aggregated to the entire 510 ha study area.

These studies show how map uncertainty is reduced as the size of the area of interest increases, although several authors only achieved reduced uncertainty with a loss of spatial resolution. Our study demonstrates that focusing monitoring efforts on changes in *aggregate* landscape AGWB-C over time could be an efficient approach to developing C payment programs related to CSA adoption. Furthermore, the methods presented in this paper show that this can be achieved without sacrificing spatial resolution, allowing for assessment of spatial variability within an aggregated area for planning and monitoring purposes. The utility of spatial analysis for project planning is underscored by our finding that targeting areas with higher C storage potential resulted in 46% larger C gains for the same area converted to CSA, compared to a random approach. However, more complex analysis would be needed to fully assess the utility of such maps for targeted project planning in practice, and it is likely results would vary by region and context.

4.2. Predicting changes in AGWB-C with CSA adoption and potential C values

Widespread adoption of CSA in this landscape could substantially increase C stocks. Agriculture is already an important component of AGWB-C storage, comprising 39% of the landscape and storing nearly 20% of all AGWB-C stocks. CSA adoption could potentially double the AGWB-C stored in agricultural land, increasing stocks in the study area by up to 46,270 tons.

Based on current market price ranges ($4–12 per ton CO_2 equivalent), the annual value of C per hectare of land converted to

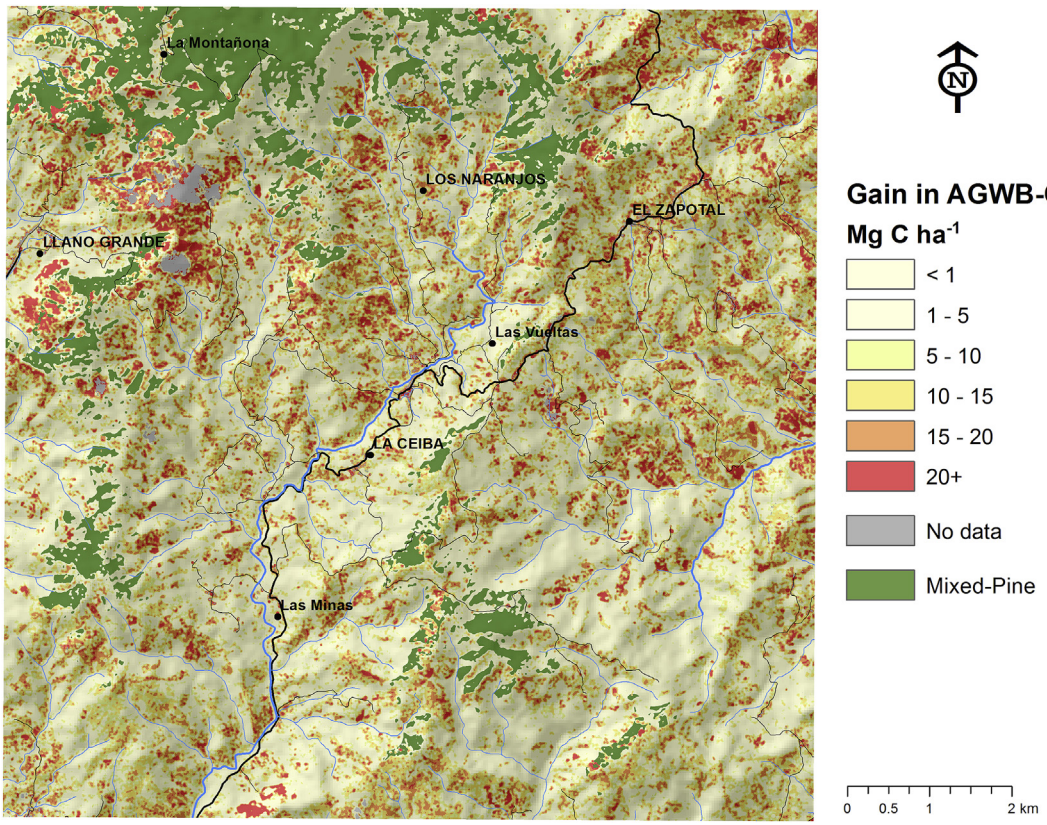

Fig. 6. Map of average expected AGWB-C density gains in the study area.

Table 6
Expected aboveground woody biomass (AGWB-C) gains for three adoption scenarios, and the potential gross value (USD) of C over 15 years at three prices for each scenario.

Adoption scenario	AGWB-C Gain[a]	CO_2 equivalent	at $4/ton		at $12/ton		at $37/ton	
	Mg	Mg	Total	Annual	Total	Annual	Total	Annual
100%	57,340	210,400	$841,600	$56,110	$2,525,000	$168,300	$7,785,000	$519,000
50% Targeted	39,110	143,500	$574,000	$38,270	$1,722,000	$114,800	$5,310,000	$354,000
50% Random	26,770	98,250	$393,000	$26,200	$1,179,000	$78,600	$3,635,000	$242,300

[a] Minimum expected measurable AGWB-C gain after accounting for map uncertainty.

CSA averages \$13–40 ha^{-1} yr^{-1}. Some studies have identified successful programs offering similar payments for watershed enhancement services provided by agroforestry and reforest ration (e.g., Kosoy et al., 2007), however others have suggested that per-hectare C payments in this range would be insufficient to incentivize small-scale farmers to adopt CSA, especially once transaction costs for farm-scale monitoring and contracting are included (Cacho et al., 2013; Henry et al., 2009; Luedeling et al., 2011).

While we estimate that per-hectare C values from CSA adoption are low, the value of C aggregated across the study area is substantial. Furthermore, we demonstrate that AGWB-C can be estimated from high-resolution satellite imagery for large areas (greater than ~250 ha) with low uncertainty, which could substantially reduce transaction costs and uncertainty associated with C monitoring across landscapes. These finding support those of other studies suggesting that C-payment programs for smallholder CSA adoption may need to be developed with groups of landholders, community-based organizations or C aggregators (e.g., Cacho et al., 2013; Henry et al., 2009). Forming C contracts with organizations rather than individual land owners could also offer a number of additional benefits, especially in the context of CSA projects, such as: increased flexibility in how CSA is promoted and incentivized; the ability to include additional C gains that may occur in non-agricultural lands (e.g., from reduced wildfires and improved fallows); and the possibility to combine C payments with incentives for additional ecosystem services provided by CSA (e.g., water funds) or civic and livelihood projects (Stringer et al., 2012). However, more work is needed to better quantify how C accountability at more aggregated scales may impact transaction costs and land use decisions.

5. Conclusions

CSA presents an opportunity to substantially increase C stocks in smallholder landscapes while simultaneously providing additional benefits, including increased resilience to an already changing climate. The per-hectare value of AGWB-C gains from CSA adoption is low, but becomes substantial when aggregated across hundreds or thousands of hectares. Monitoring at this scale using satellite imagery could substantially reduce transaction costs, however a tendency in the literature to report only plot-scale errors (e.g., RMSE) without exploring the aggregated error of AGWB-C maps is

likely limiting the operationalization of satellite-based monitoring approaches.

Our findings demonstrate that high-resolution satellite imagery can be used to accurately monitor aggregate AGWB-C at the watershed to landscape scale (100~10,000 ha) in highly heterogeneous smallholder landscapes. Comparing the few studies that have quantified the uncertainty of AGWB-C and C emissions at multiple scales with our study, we conclude that areas of 200–300 ha may be an appropriate minimum scale at which to monitor aggregated C stocks with low uncertainty (i.e., < 5%) using optical satellite imagery. Texture variables are at least as important as vegetation indices to develop AGWB-C prediction models with high spatial resolution passive optical satellite imagery, and mapping AGWB-C at high resolution could considerably increase C gains per unit area converted to CSA by allowing projects to efficiently target low-biomass areas.

Landscape-scale accountability of C, supported by satellite-based methods such as that presented in this study, can reduce costs and uncertainty associated with C monitoring. Such an approach can thereby overcome some of the methodological concerns hindering the inclusion of CSA in international and voluntary C agreements, and support both market and non-market mechanisms to incentivize widespread CSA adoption in heterogeneous smallholder landscapes globally.

Acknowledgements

This work was supported by funding from the United States Agency for International Development (USAID) [award number AID-519-A-12-00002-00]. USAID had no role in the study design, collection, analysis and interpretation of data, writing of the manuscript or the decision to submit the article for publication. We express our great thanks to the office of the Association of Municipalities of La Mancomunidad La Montañona, the Natural History Museum of El Salvador (MUHNES), the mayors' offices of La Mancomunidad La Montañona, Rolando Barillas and the hardworking members of the field crew of Las Vueltas and El Zapotal.

Appendix A. Supplementary materials

Supplementary materials related to this article can be found at http://dx.doi.org/10.1016/j.jenvman.2017.07.039.

References

Asner, G.P., Powell, G.V.N., Mascaro, J., Knapp, D.E., Clark, J.K., Jacobson, J., Kennedy-Bowdoin, T., Balaji, A., Paez-Acosta, G., Victoria, E., Secada, L., Valqui, M., Hughes, R.F., 2010. High-resolution forest carbon stocks and emissions in the Amazon. Proc. Natl. Acad. Sci. U. S. A. 107, 16738–16742. http://dx.doi.org/10.1073/pnas.1004875107.

Cacho, O.J., Lipper, L., Moss, J., 2013. Transaction costs of carbon offset projects: a comparative study. Ecol. Econ. 88, 232–243. http://dx.doi.org/10.1016/j.ecolecon.2012.12.008.

Castillo-Santiago, M.A., Ricker, M., de Jong, B.H.J., 2010. Estimation of tropical forest structure from SPOT-5 satellite images. Int. J. Remote Sens. 31, 2767–2782. http://dx.doi.org/10.1080/01431160903095460.

Chhatre, A., Agrawal, A., 2009. Trade-offs and synergies between carbon storage and livelihood benefits from forest commons. Proc. Natl. Acad. Sci. 106, 17667–17670. http://dx.doi.org/10.1073/pnas.0905308106.

Dagang, A.B.K., Nair, P., 2003. Silvopastoral research and adoption in Central America: recent findings and recommendations for future directions. Agrofor. Syst. 59, 149–155. http://dx.doi.org/10.1007/BF00115736.

Eckert, S., 2012. Improved forest biomass and carbon estimations using texture measures from WorldView-2 satellite data. Remote Sens. 4, 810–829. http://dx.doi.org/10.3390/rs4040810.

ESRI, 2011. ArcGIS Desktop. Release 10.1, Redlands, CA.

Exelis Visual Information Solutions, 2010. ENVI 5.0. Boulder, CO.

Fazakas, Z., Nilsson, M., Olsson, H., 1999. Regional forest biomass and wood volume estimation using satellite data and ancillary data. Agric. For. Meteorol. 98–99, 417–425. http://dx.doi.org/10.1016/S0168-1923(99)00112-4.

Fuchs, H., Magdon, P., Kleinn, C., Flessa, H., 2009. Estimating aboveground carbon in a catchment of the Siberian forest tundra: combining satellite imagery and field inventory. Remote Sens. Environ. 113, 518–531. http://dx.doi.org/10.1016/j.rse.2008.07.017.

García, M., Riaño, D., Chuvieco, E., Danson, F.M., 2010. Estimating biomass carbon stocks for a Mediterranean forest in central Spain using LiDAR height and intensity data. Remote Sens. Environ. 114, 816–830. http://dx.doi.org/10.1016/j.rse.2009.11.021.

Gibbs, H.K., Brown, S., Niles, J.O., Foley, J.A., 2007. Monitoring and estimating tropical forest carbon stocks: making REDD a reality. Environ. Res. Lett. 2, 1–13. http://dx.doi.org/10.1088/1748-9326/2/4/045023.

Goetz, S., Baccini, A., Laporte, N., Johns, T., Walker, W., Kellndorfer, J., Houghton, R., Sun, M., 2009. Mapping and monitoring carbon stocks with satellite observations: a comparison of methods. Carbon Balance Manag. 4, 1–7. http://dx.doi.org/10.1186/1750-0680-4-2.

Goetz, S., Dubayah, R., 2011. Advances in remote sensing technology and implications for measuring and monitoring forest carbon stocks and change. Carbon Manag. 2, 231–244. http://dx.doi.org/10.4155/cmt.11.18.

Gómez-Castro, H., Pinto-Ruiz, R., Guevara-Hernández, F., Gonzalez-Reyna, A., 2010. Estimaciones de biomasa aérea y carbono almacenado en Gliricidia sepium (lam.) y Leucaena leucocephala (jacq.) y su aplicación en sistemas silvopastoriles. Inf. Técnica Econ. Agrar. 106, 256–270.

Harley, R., Riddell, M., Ndobe, S.N., 2012. REDD+ beyond carbon: insights from a community payments for ecosystem services project in Cameroon. Bioclimate Research and Development, Edinburgh, Scotland, UK.

Harvey, C. a., Chacón, M., Donatti, C.I., Garen, E., Hannah, L., Andrade, A., Bede, L., Brown, D., Calle, A., Chará, J., Clement, C., Gray, E., Hoang, M.H., Minang, P., Rodríguez, A.M., Seeberg-Elverfeldt, C., Semroc, B., Shames, S., Smukler, S., Somarriba, E., Torquebiau, E., van Etten, J., Wollenberg, E., 2013. Climate-smart landscapes: opportunities and challenges for integrating adaptation and mitigation in tropical agriculture. Conserv. Lett. 0, 1–14. http://dx.doi.org/10.1111/conl.12066.

Hellin, J., Welchez, L.A., Cherrett, I., 1999. The Quezungual System: an indigenous agroforestry system from western Honduras. Agrofor. Syst. 46, 229–237. http://dx.doi.org/10.1023/A:1006217201200.

Henry, M., Tittonell, P., Manlay, R.J., Bernoux, M., Albrecht, A., Vanlauwe, B., 2009. Biodiversity, carbon stocks and sequestration potential in aboveground biomass in smallholder farming systems of western Kenya. Agric. Ecosyst. Environ. 129, 238–252. http://dx.doi.org/10.1016/j.agee.2008.09.006.

Hughes, R., Kauffman, J., Jaramillo, V., 1999. Biomass, carbon and nutrient dynamics of secondary forests in a humid tropical region of Mexico. Ecology 80, 1892–1907. http://dx.doi.org/10.2307/176667.

Jensen, J.R., 2005. Introductory Digital Image Processing: a Remote Sensing Perspective. Prentice Hall Inc., Upper Saddle River, N.J.

Kayitakire, F., Hamel, C., Defourny, P., 2006. Retrieving forest structure variables based on image texture analysis and IKONOS-2 imagery. Remote Sens. Environ. 102, 390–401. http://dx.doi.org/10.1016/j.rse.2006.02.022.

Kearney, S.P., Smukler, S.M., 2016. Determining greenhouse gas emissions and removals associated with land-use and land-cover change. In: Rosenstock, T.S., Rufino, M.C., Butterbach-Bahl, K., Wollenberg, E., Richards, M. (Eds.), Methods for Measuring Greenhouse Gas Balances and Evaluating Migration Options in Smallholder Agriculture. Springer. http://dx.doi.org/10.1007/978-3-319-29794-1_3.

Kosoy, N., Martinez-Tuna, M., Muradian, R., Martinez-Alier, J., 2007. Payments for environmental services in watersheds: insights from a comparative study of three cases in Central America. Ecol. Econ. 61, 446–455. http://dx.doi.org/10.1016/j.ecolecon.2006.03.016.

Lorenz, K., Lal, R., 2014. Soil organic carbon sequestration in agroforestry systems. A review. Agron. Sustain. Dev. 34, 443–454. http://dx.doi.org/10.1007/s13593-014-0212-y.

Luedeling, E., Sileshi, G., Beedy, T., Dietz, J., 2011. Carbon sequestration potential of agroforestry systems. Adv. Agrofor., Adv. Agrofor. 8, 61–83. http://dx.doi.org/10.1007/978-94-007-1630-8.

Lumley, T., 2009. Leaps: Regression Subset Selection.

Lusiana, B., van Noordwijk, M., Johana, F., Galudra, G., Suyanto, S., Cadisch, G., 2014. Implications of uncertainty and scale in carbon emission estimates on locally appropriate designs to reduce emissions from deforestation and degradation (REDD+). Mitig. Adapt. Strateg. Glob. Chang. 19, 757–772. http://dx.doi.org/10.1007/s11027-013-9501-z.

Maindonald, J.H., Braun, W.J., 2015. DAAG: Data Analysis and Graphics Data and Functions. R Package Version 1.22.

Marinidou, E., Finegan, B., Jiménez-Ferrer, G., Delgado, D., Casanoves, F., 2013. Concepts and a methodology for evaluating environmental services from trees of small farms in Chiapas, México. J. Environ. Manage. 114, 115–124. http://dx.doi.org/10.1016/j.jenvman.2012.10.046.

MARN (Ministry of Environment and Natural Resources, El Salvador), 2013. Datos históricos de precipitación: estaciónes G-12 de Concepción Quezaltepeque y G-7 de Arcatao (1971-2012). Pers. Commun.

Mascaro, J., Asner, G.P., Muller-Landau, H.C., Van Breugel, M., Hall, J., Dahlin, K., 2011a. Controls over aboveground forest carbon density on Barro Colorado Island, Panama. Biogeosciences 8, 1615–1629. http://dx.doi.org/10.5194/bg-8-1615-2011.

Mascaro, J., Detto, M., Asner, G.P., Muller-Landau, H.C., 2011b. Evaluating uncertainty in mapping forest carbon with airborne LiDAR. Remote Sens. Environ. 115, 3770–3774. http://dx.doi.org/10.1016/j.rse.2011.07.019.

Nichol, J.E., Sarker, M.L.R., 2011. Improved biomass estimation using the texture

parameters of two high-resolution optical sensors. IEEE Trans. Geosci. Remote Sens. 49, 930–948. http://dx.doi.org/10.1109/TGRS.2010.2068574.
Okubo, S., Parikesit, D.M., Harashina, K., Takeuchi, K., Umezaki, M., 2010. Land use/cover classification of a complex agricultural landscape using single-dated very high spatial resolution satellite-sensed imagery. Can. J. Remote Sens. 36, 722–736. http://dx.doi.org/10.5589/m11-010.
Palmer, M., 2003. Propagation of Uncertainty Through Mathematical Operations. MIT School-wide Modular Program for Fluid Mechanics - Experimental Techniques, pp. 1–7 [WWW Document]. http://web.mit.edu/fluids-modules/www/exper_techniques/2.Propagation_of_Uncertaint.pdf (Accessed 16 June 2015).
Pauli, N., Barrios, E., Conacher, A.J., Oberthür, T., 2011. Soil macrofauna in agricultural landscapes dominated by the Quesungual Slash-and-Mulch Agroforestry System, western Honduras. Appl. Soil Ecol. 47, 119–132. http://dx.doi.org/10.1016/j.apsoil.2010.11.005.
Pebesma, E.J., 2004. Multivariable geostatistics in S: the gstat package. Comput. Geosci. 30, 683–691. http://dx.doi.org/10.1016/j.cageo.2004.03.012.
Pelletier, J., Kirby, K.R., Potvin, C., 2012. Significance of carbon stock uncertainties on emission reductions from deforestation and forest degradation in developing countries. For. Policy Econ 24, 3–11. http://dx.doi.org/10.1016/j.forpol.2010.05.005.
R Core Team, 2016. R: a Language and Environment for Statistical Computing. Vienna, Austria.
Ravindranath, N., Ostwald, M., 2008. Carbon Inventory Methods: Handbook for Greenhouse Gas Inventory, Carbon Mitigation and Roundwood Production Projects, 29th ed. Springer, Netherlands.
Rosenstock, T.S., Rufiano, M.C., Butterbach-Bahl, K., Wollenberg, E., Richards, M., 2016. Methods for Measuring Greenhouse Gas Balances and Evaluating Mitigation Options in Smallholder Agriculture, first ed. Springer International Publishing.
Saatchi, S.S., Harris, N.L., Brown, S., Lefsky, M., Mitchard, E.T.A., Salas, W., Zutta, B.R., Buermann, W., Lewis, S.L., Haga, S., White, L., Silman, M., Morel, A., 2011. Benchmark map of forest carbon stocks in tropical regions across three continents. Proc. Natl. Acad. Sci. U. S. A. 108, 9899–9904. http://dx.doi.org/10.1073/pnas.1019576108.
Sarker, L.R., Nichol, J.E., 2011. Improved forest biomass estimates using ALOS AVNIR-2 texture indices. Remote Sens. Environ. 115, 968–977. http://dx.doi.org/10.1016/j.rse.2010.11.010.
Scherr, S.J., Shames, S., Friedman, R., 2012. From climate-smart agriculture to climate-smart landscapes. Agric. Food Secur 1, 12. http://dx.doi.org/10.1186/2048-7010-1-12.
Sexton, J.O., Noojipady, P., Anand, A., Song, X., Mcmahon, S., Huang, C., Feng, M., Channan, S., Townshend, J.R., 2015. A model for the propagation of uncertainty from continuous estimates of tree cover to categorical forest cover and change. Remote Sens. Environ. 156, 418–425. http://dx.doi.org/10.1016/j.rse.2014.08.038.
Shepherd, K.D., Shepherd, G., Walsh, M.G., 2015. Land health surveillance and response: a framework for evidence-informed land management. Agric. Syst. 132, 93–106. http://dx.doi.org/10.1016/j.agsy.2014.09.002.
Sprugel, D.G., 1983. Correcting for bias in log-transformed allometric equations. Ecology 64, 209–210. http://dx.doi.org/10.2307/1937343.
Steenwerth, K.L., Hodson, A.K., Bloom, A.J., Carter, M.R., Cattaneo, A., Chartres, C.J., Hatfield, J.L., Henry, K., Hopmans, J.W., Horwath, W.R., Jenkins, B.M., Kebreab, E., Leemans, R., Lipper, L., Lubell, M.N., Msangi, S., Prabhu, R., Reynolds, M.P., Sandoval Solis, S., Sischo, W.M., Springborn, M., Tittonell, P., Wheeler, S.M., Vermeulen, S.J., Wollenberg, E.K., Jarvis, L.S., Jackson, L.E., 2014. Climate-smart agriculture global research agenda: scientific basis for action. Agric. Food Secur 3, 11. http://dx.doi.org/10.1186/2048-7010-3-11.
Stringer, L.C., Dougill, A.J., Thomas, A.D., Spracklen, D.V., Chesterman, S., Speranza, C.I., Rueff, H., Riddell, M., Williams, M., Beedy, T., Abson, D.J., Klintenberg, P., Syampungani, S., Powell, P., Palmer, A.R., Seely, M.K., Mkwambisi, D.D., Falcao, M., Sitoe, A., Ross, S., Kopolo, G., 2012. Challenges and opportunities in linking carbon sequestration, livelihoods and ecosystem service provision in drylands. Environ. Sci. Policy 19–20, 121–135. http://dx.doi.org/10.1016/j.envsci.2012.02.004.
Suárez, D., 2002. Cuantificación y valoraicón económica del servicio ambiental almacenamiento de carbono en sistemas agroforestales de café en la Comarca Yassica Sur. CATIE, Matagalpa, Nicaragua.
Tsui, O.W., Coops, N.C., Wulder, M. a., Marshall, P.L., 2013. Integrating airborne LiDAR and space-borne radar via multivariate kriging to estimate above-ground biomass. Remote Sens. Environ. 139, 340–352. http://dx.doi.org/10.1016/j.rse.2013.08.012.
Turnhout, E., Gupta, A., Weatherley-Singh, J., Vijge, M.J., de Koning, J., Visseren-Hamakers, I.J., Herold, M., Lederer, M., 2017. Envisioning REDD+ in a post-Paris era: between evolving expectations and current practice. WIREs Clim. Chang. 8, 1–13. http://dx.doi.org/10.1002/wcc.425.
US Interagency Working Group on the Social Cost of Carbon, 2015. Technical Support Document: -Technical Update of the Social Cost of Carbon for Regulatory Impact Analysis-U-nder Executive Order 12866. July 2015 Revision.
Verchot, L.V., Noordwijk, M., Kandji, S., Tomich, T., Ong, C., Albrecht, A., Mackensen, J., Bantilan, C., Anupama, K.V., Palm, C., 2007. Climate change: linking adaptation and mitigation through agroforestry. Mitig. Adapt. Strateg. Glob. Chang. 12, 901–918. http://dx.doi.org/10.1007/s11027-007-9105-6.
Wilson, J.P., Gallant, J.C., 2000. Digital terrain analysis. In: Wilson, J.P., Gallant, J.C. (Eds.), Terrain Analysis: Principles and Applications. John Wiley & Sons, New York, pp. 1–27. http://dx.doi.org/10.5194/hess-4-225-2000.
Yarbrough, L.D., Easson, G., 2005. Quickbird 2 Tasseled Cap Transform Coefficients: a Comparison of Derivation Methods, in: Pecora 16 Symposium "Global Priorities in Land Remote Sensing." (Sioux Falls, South Dakota, USA).
Zolkos, S.G., Goetz, S.J., Dubayah, R., 2013. A meta-analysis of terrestrial above-ground biomass estimation using lidar remote sensing. Remote Sens. Environ. 128, 289–298. http://dx.doi.org/10.1016/j.rse.2012.10.017.